

A NUMERICAL CONTINUOUS MODEL FOR THE HYDRODYNAMICS OF FLUID PARTICLE SYSTEMS

J.B. RITZ* AND J.P. CALTAGIRONE

MASTER-ENSCPB, Modélisation Avancée des Systèmes Thermiques et des Écoulements Réels,
Ecole Nationale Supérieure de Chimie et de Physique de Bordeaux, Avenue Pey-Berland, BP 108,
33402 Talence Cedex, France

SUMMARY

In order to understand the hydrodynamic interactions that can appear in a fluid particle motion, an original method based on the equations governing the motion of two immiscible fluids has been developed. These momentum equations are solved for both the fluid and solid phases. The solid phase is assumed to be a fluid phase with physical properties, such as its behaviour can be assimilated to that of pseudo-rigid particles. The only unknowns are the velocity and the pressure defined in both phases. The unsteady two-dimensional momentum equations are solved by using a staggered finite volume formulation and a projection method. The transport of each particle is solved by using a second-order explicit scheme. The physical model and the numerical method are presented, and the method is validated through experimental measurements and numerical results concerning the flow around a circular cylinder. Good agreement is observed in most cases. The method is then applied to study the trajectory of one settling particle initially off-centred between two parallel walls and the corresponding wake effects. Different particle trajectories related to particulate Reynolds numbers are presented and commented. A two-body interaction problem is investigated too. This method allows the simulation of the transport of particles in a dilute suspension in reasonable time. One of the important features of this method is the computational cost that scales linearly with the number of particles. Copyright © 1999 John Wiley & Sons, Ltd.

KEY WORDS: fluid particle motion; direct numerical simulation; finite volume method; wake effects; sedimentation

1. INTRODUCTION

The motion of solid particles dispersed in a fluid phase is encountered in an increasing number of industrial processes. It is found, for instance, in petroleum extraction, coal, filtration and solid rocket propellant manufacturing. The challenge is to model such motions. In order to close the averaged equations of the global motion in a Euler–Euler approach or to define the transfer functions in a Euler–Lagrange approach, some coefficients that quantify the interactions between the two phases [1] must be defined. No matter the approach, local hydrodynamic interactions, such as particle–fluid, particle–particle and particle–wall interactions, must be known. In the literature, many empirical relations and data correlations can be found for coupling or drag coefficients depending on the nature of the motion [2]. This fact points out that all the hydrodynamic interactions must be known *a priori*. For simple cases, these relations are well-adapted and lead to good results. Unfortunately, most industrial processes

* Correspondence to: Laboratoire MASTER-ENSCPB, Avenue Pey-Berland, BP 108, 33402 Talence Cedex, France.

do not verify these classical assumptions: semi-dilute or concentrated suspensions with high velocities, unsteady and non-uniform flows, walls and singularities, particle size larger than Kolmogorov scales, . . . In most cases, the flow regime induces irreversible and non-linear hydrodynamic interactions. As a result, the knowledge of these hydrodynamic interactions and their importance for all flow configurations are fundamental to improve on the global models described above. The local phenomena can be predicted by calculating the motion of dispersed particles in a surrounding fluid with the smallest number of hypotheses. This approach is called direct simulation. It is a deterministic approach. The forces acting on the surface of the particles are evaluated directly with no averaging or approximation and the flow evolves according to the motion of these particles. The same can be said of turbulence phenomena, where direct simulation allows the development of new turbulence models based on the knowledge of every flow scale. In the present case, the modelling of the motion of a few particles (as many as possible) can serve as a guideline for understanding more complicated systems and can help in quantifying the full hydrodynamic interactions during the motion. In other words, to understand and describe the macroscopic flow of a suspension, one must take into account the microscopic properties and the interactions of the microstructure.

The development of a direct simulation method is a difficult task. The method should allow for a large number of moving particles and should be able to cope with the discontinuity between the two phases so that the local action of the flow on the particles is accurately predicted. Particle surface can be regarded as a boundary or an interface. Two different meshing strategies are possible. The first one, normally used with the finite element method, consists of taking into account the relative position of the particles as a boundary of the fluid domain. Remeshing is then needed at each time step. Alternatively, one can use a fixed grid and track the surface of the moving particles over time. This is the approach often encountered with the finite volume or the finite difference method.

Concerning the use of moving grids, Hu *et al.* [3,4] derived a method based on the Navier–Stokes equations for the fluid and Newton's equations for the solid particles. They can predict the respective motion of two two-dimensional particles including the drafting, kissing and tumbling (DKT) phenomenon observed by Fortes *et al.* [5]. The action of the fluid on the particles is obtained from experimental curves and empirical formulations [3] or evaluated explicitly by an integration along the surface of the particles [6,7]. This approach necessitates a remeshing procedure and the mapping of the flow fields from the old mesh onto the new mesh. To overcome these difficulties and the inherent computational cost when the number of particles becomes large or a three-dimensional computational domain is considered, Johnson and Tezduyar [8,9] have developed an interesting strategy based on the deforming spatial domain/space–time procedure developed by Tezduyar *et al.* [10]. The domain is composed of deformable finite elements. Remeshing becomes necessary when the grid gets too distorted. With this approach, they can simulate the motion of settling particles in three dimensions and predict the DKT phenomenon [8]. They were able to simulate as many as 100 particles in the three-dimensional case [9]. Recently, Glowinski *et al.* [11] proposed to simulate the motion of two-dimensional rigid particles in a suspending fluid using a finite element based fictitious domain method. The interface between the solid and fluid is defined by control points, on each of which a kinematic condition is imposed using a Lagrange multiplier. The motion of these control points is governed by the action of the fluid on the surface of the particles. The interest of this method is that it relies on a fixed mesh. No remeshing is needed, which is an interesting feature especially when the number of particles increases and a large portion of the fluid space is filled with particles.

The scope of this paper is to present a new procedure based on a fixed, structured and uniform grid and the finite volume method. The definition of a continuous hydrodynamic model that has been adopted here leads to a unique system of equations for both phases. This approach does not need remeshing and seeks the solution to the problem in a coupled manner. The remainder of the paper is as follows. First the physical model and the numerical method are presented in Sections 2 and 3 respectively. The method is then validated by comparing the numerical results obtained for the flow around a circular cylinder with those found in the literature. The motion of settling particles in a closed channel is studied in detail to characterise particle–fluid, particle–wall and particle–particle interactions, and special attention is given to wake effects in Section 4. Finally, conclusions are drawn in Section 5.

2. GOVERNING EQUATIONS

We consider the incompressible flow of two non-miscible Newtonian fluids separated by a material interface. One of the fluids is dispersed into the other. Let $t \in [0, T]$ and let D be the two-dimensional computational domain of boundary ∂D . In the sequel, D_f , ρ_f and μ_f respectively represent the domain, the density and the viscosity of the continuous phase, and D_d , ρ_d and μ_d the domain, the density and the viscosity of the dispersed phase. The interface between the two fluids is denoted by Σ and the velocity and the normal unit vector are respectively denoted by V_i and n_i (see Figure 1).

The incompressible momentum equations for the two non-miscible fluids in D are formulated in terms of velocity $\mathbf{V}(\mathbf{x}, t)$ and pressure $p(\mathbf{x}, t)$, where \mathbf{x} is the position vector, $\mathbf{x} = x\mathbf{i} + y\mathbf{j}$ in a Cartesian co-ordinate system, where \mathbf{i} and \mathbf{j} are the unit vectors parallel to the co-ordinate axes:

Mass conservation:

$$\frac{d}{dt} \iiint_D \rho \, dv = \iiint_D \left(\frac{\partial \rho}{\partial t} + \nabla \cdot (\rho \mathbf{V}) \right) dv + \iint_{\Sigma} [[\rho(\mathbf{V} - \mathbf{V}_i)]] \cdot \mathbf{n}_i \, d\Sigma, \tag{1}$$

Momentum conservation:

$$\begin{aligned} & \iiint_D \left(\frac{\partial}{\partial t} (\rho \mathbf{V}) + \nabla \cdot (\rho \mathbf{V} \otimes \mathbf{V}) \right) dv \\ &= \iiint_D (\rho \mathbf{f} + \nabla \cdot \bar{\bar{\sigma}}) \, dv - \iint_{\Sigma} [[\rho \mathbf{V} \otimes (\mathbf{V} - \mathbf{V}_i) - \bar{\bar{\sigma}}]] \cdot \mathbf{n}_i \, d\Sigma, \end{aligned} \tag{2}$$

where $[[\cdot]]$ denotes the jump at the interface Σ ; $\bar{\bar{\sigma}}$ is the Cauchy tensor. In the case of a contact surface between the two immiscible fluids without surface tension, the jump conditions are as follows:

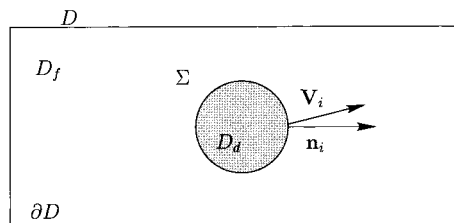


Figure 1. Definition of the domain that contains a surface of discontinuity Σ .

$$[[\mathbf{V}]] \cdot \mathbf{n}_i = 0. \quad (3)$$

$$[[\bar{\boldsymbol{\sigma}}]] \cdot \mathbf{n}_i = 0. \quad (4)$$

These respectively imply the continuity of the normal velocity and the stress vector through the interface. The equations defined above allow the simulation of the motion of two immiscible fluids. The idea now is to modify the constitutive law of the dispersed phase to describe a pseudo-rigid behaviour.

2.1. Specific constitutive law for the dispersed phase

To define the constitutive law of the dispersed phase, we assume that the solid phase D_d is a fluid phase with a very high viscosity and look for a constitutive law that is similar to that of a pseudo-rigid non-elastic particle.

Let us look in more detail at the momentum equations when the viscosity of the dispersed phase D_d is very high compared with that of the continuous phase D_f . First, let us consider the stress tensor in the dispersed phase. This term is well-defined and has a finite dimension. It represents the continuity of the stress field at the interface of a particle. As a Newtonian law is used over the whole domain, we write:

$$\bar{\boldsymbol{\tau}} = \mu_d(\nabla\mathbf{V} + \nabla\mathbf{V}'). \quad (5)$$

If now the viscosity μ_d increases very strongly, then the rate-of-strain tensor term tends to zero in the particle, which presents a way to characterise the pseudo-rigid region D_d . The velocity for this phase, \mathbf{V}_M is then composed of two velocities, a translational velocity defined as the velocity of the centre of gravity G of the particle and the velocity due to the rotational velocity $\boldsymbol{\Omega}_G$: $\mathbf{V}_M = \mathbf{V}_G + \mathbf{M}\mathbf{G} \wedge \boldsymbol{\Omega}_G$, where M is a point included in the region D_d . By tracking the regions of the domain where the rate-of-strain tensor tends to zero, we then obtain a characterisation of the motion of the particles. Two conditions are to be respected in D , let alone that of incompressibility:

$$\nabla \cdot \mathbf{V} = 0 \quad \text{in } D_f, \quad (6)$$

and that of indeformability, which guarantees that the particle motion is rigid:

$$D_{ij} \rightarrow 0 \quad \text{in } D_d. \quad (7)$$

It is important to stress that this model is valid only if the continuity of the stress tensor is satisfied at the interface. For instance, if the rate-of-strain tensor is equal to zero, we do not have the continuity across the interface of the stress vector. Consequently, to ensure that the dispersed phase is pseudo-rigid, it is assumed that:

$$t_c(\bar{D}) \gg t_c\left(\frac{d_p}{V_p}\right), \quad (8)$$

i.e. it is assumed that the characteristic time representing the deformation of the particle will be larger than the flow characteristic time.

With this formulation, no kinematic condition is needed at the fluid–solid interface. The continuity of the normal velocity and the stress tensor at the interface is implicitly satisfied. It is interesting to note that the numerical discretisation ensures the continuity of the tangential velocity too. There is no possibility to allow for slip condition at the interface.

It is straightforward to extend the methodology to the case of many particles. In this case, D_{d_i} , ∂D_{d_i} and V_{d_i} respectively denote the domain, the boundary and the volume of the i th

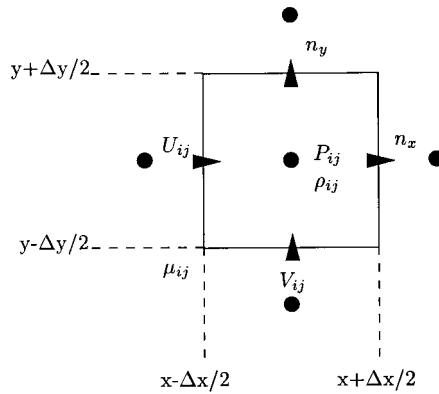


Figure 2. A staggered mesh in two dimensions.

dispersed particle. The position of the i th particle is determined by the position of its centre $\mathbf{r}_i(\mathbf{x}_i, t)$ (with $\mathbf{r}_i = x_i\mathbf{i} + y_i\mathbf{j}$) and its rotational angle $\theta_i(t)$. Its motion is determined by the velocity $\mathbf{V}_i(\mathbf{x}_i, t)$ and the angular velocity $\Omega_i(\theta_i, t)$. The velocity of the particle centre of gravity is evaluated by integrating the velocity field defined for the dispersed phase. The angular velocity is evaluated by integrating the vorticity field for the dispersed phase. Finally, the following model is obtained:

$$\iiint_D \left(\frac{\partial}{\partial t} (\rho \mathbf{V}) + \nabla \cdot (\rho \mathbf{V} \otimes \mathbf{V}) \right) dv = \iiint_D (-\nabla p + \nabla \cdot [2\mu \bar{\bar{D}}] + \rho \mathbf{g}) dv,$$

$$\mathbf{V}_i = \frac{d\mathbf{r}_i}{dt} = \frac{1}{V_{d_i}} \iiint_{D_{d_i}} \mathbf{V} dv,$$

$$\Omega_i = \frac{d\theta_i}{dt} = \frac{1}{V_{d_i}} \iiint_{D_{d_i}} \frac{1}{2} \nabla \wedge \mathbf{V} dv,$$

$$\bar{\bar{D}} = \frac{1}{2} (\nabla \mathbf{V} + \nabla \mathbf{V}^t) \quad \forall \mathbf{V} \in D_f,$$

$$\bar{\bar{D}} \rightarrow 0 \quad \forall \mathbf{V} \in D_d.$$

3. NUMERICAL METHODS

3.1. Spatial discretisation

The equations above are discretised using the finite volume method. To transform the differential equations into algebraic equations, the conservation equations are integrated over finite volumes $\Delta V = \Delta x \Delta y$ in a fixed co-ordinate system. A staggered grid based version of the MAC method developed by Harlow and Welch [12] was used for the discretisation of the velocity and pressure. As sketched in Figure 2, the normal velocity components are staggered relative to the location of the pressure variables, so that the cells are centred on the pressure nodes and the velocities are located on the cell faces.

3.2. Numerical treatment of the discontinuities

In the present approach, we consider that the discontinuity at the interface of physical quantities, such as the viscosity and the density, corresponds to a continuous function with a very steep slope. This simplistic assumption leads to an approximation of the problem that is fairly accurate and easy to implement. With this model, the volume fraction is defined as:

$$\begin{aligned} F_{ij} &= 0 & \text{in } D_f, \\ F_{ij} &= 1 & \text{in } D_d, \end{aligned} \quad (9)$$

and $0 < F_{ij} < 1$ in the hybrid cell containing the discontinuities. The value of the volume fraction depends on the position of the discontinuity. The evaluation of the volume fraction allows the calculation of the values of the density and the viscosity in the whole domain by a volume averaging technique. For the density, we write:

$$\rho_{ij} = \rho_d(1 - F_{ij}) + \rho_f F_{ij}, \quad (10)$$

which is linear when arithmetic interpolation is used.

For the treatment of the viscosity, another strategy is proposed because the viscosity of the dispersed phase is so large with respect to that of continuous phase that a simple averaging technique would yield this viscosity whatever the value of the volume fraction.

$$\mu_{ij} = \mu_d(1 - F_{ij}) + \mu_f F_{ij} \simeq \mu_d. \quad (11)$$

In place, we suggest the use of another averaging technique based on the conservation of the viscous flux through the interface with respect to its position in the cell.

More precisely, we define in the cell containing the discontinuity some equivalent physical properties that ensure two conditions. First, the local conservation of the flux through the cell faces and then, the conservation of the flux through the interface, which is included in the cell (Figure 3). This averaging technique can be easily extended to the two-dimensional case. The grid nodes for the viscosity field are defined at the corner of the scalar control volume (Figure 2).

$$\mu_{ij} = \frac{\mu_d \mu_f}{(1 - F_{ij})\mu_d + F_{ij}\mu_f}. \quad (12)$$

The underlying momentum equations can be solved with the method used for the solution of single phase fluid flow problems. For each phase, the physical quantities are constant during a time step. The only unknowns are the velocity and the pressure.

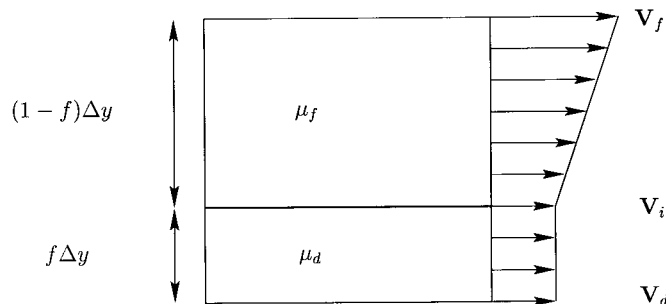


Figure 3. Simple shear at the vicinity of the solid–fluid interface.

3.3. Solution method

The solution of the momentum equations is carried out using a variant of the time splitting method of Goda [13], based on the method of Chorin [14]. The time splitting method is a method based on the decomposition of Navier–Stokes operators. First, the Navier–Stokes equations are solved to find an intermediate velocity field $\tilde{\mathbf{V}}$, which does not satisfy the incompressibility condition:

$$\begin{cases} \rho^n \left(\frac{\tilde{\mathbf{V}} - \mathbf{V}^n}{\Delta t} + (\mathbf{V}^n \cdot \nabla) \tilde{\mathbf{V}} \right) = -\nabla p^n + \nabla \cdot [\mu^n (\nabla \tilde{\mathbf{V}} + \nabla \tilde{\mathbf{V}}^t)] + (\rho^n - \rho_f^n) \mathbf{g}, \\ \tilde{\mathbf{V}}|_{\partial D} = \mathbf{0}. \end{cases} \quad (13)$$

This velocity field is then projected onto a divergence-free subspace:

$$\begin{cases} \frac{\mathbf{V}^{n+1} - \tilde{\mathbf{V}}}{\Delta t} + \frac{1}{\rho^n} \nabla (p^{n+1} - p^n) = \mathbf{0}, \\ \mathbf{V}^{n+1} \cdot \mathbf{n}|_{\partial D} = 0, \\ \nabla \cdot \mathbf{V}^{n+1}|_D = 0. \end{cases} \quad (14)$$

This projection step implies the solution of a Poisson equation applied to the pressure variation. The pressure field is zero at the initial time step.

$$\begin{cases} \nabla \cdot \nabla \phi^{n+1} = \nabla \cdot \tilde{\mathbf{V}}, \\ \frac{\partial \phi^{n+1}}{\partial n} \Big|_{\partial D} = 0, \\ \nabla \phi^{n+1} = \frac{\Delta t}{\rho^n} \nabla (p^{n+1} - p^n). \end{cases} \quad (15)$$

The following discretisation schemes are used: a third-order QUICK scheme [15] for the treatment of the convective terms, a second-order central difference scheme for the diffusive terms, and a second-order implicit Gear scheme for the transient terms [16]. In classical projection methods, the first step is solved explicitly [13]. In this work, implicit solution is preferred because such a scheme is unconditionally stable and does not necessitate a time step restrictive condition. With an explicit scheme, the large values of the viscosity in the dispersed phase would call for too small time steps to ensure its convergence. An implicit method is also employed for the solution of the Poisson equation. The two non-symmetric linear systems (13) and (15) are solved efficiently using the BiCGSTAB method proposed by Van der Vorst [17] with a Jacobi preconditioner. The transport of the particles in the fluid phase is handled with a second-order time scheme, where \mathbf{V}^{n+1} and \mathbf{V}^n denote the velocities of the particle's centre of gravity obtained from the momentum equations in the solid phase at the time step (n) and ($n + 1$).

$$\frac{\Delta \mathbf{r}_i^{n+1}}{\Delta t} = \frac{1}{2} (\mathbf{V}^n + \mathbf{V}^{n+1}). \quad (16)$$

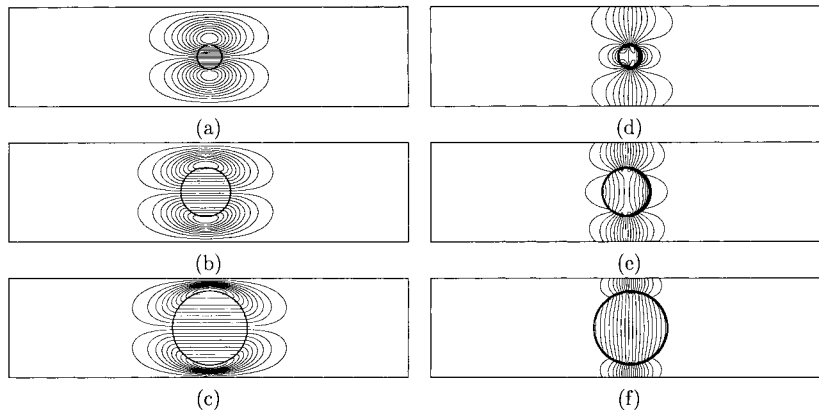


Figure 4. Typical particle motion between two parallel walls in Stokes flow: streamlines (a), (b) and (c); and isobars (d), (e) and (f) for different particle diameters.

A condition on the size of the time step is given by the following Courant–Friedrich–Lewy (CFL) number, where (u, v) represent the velocity at the interface:

$$\text{CFL} = \max_{(x)} \left(\frac{|u|}{\Delta x}, \frac{|v|}{\Delta y} \right). \quad (17)$$

This condition is needed because of the use of an explicit scheme to transport particles. In this work, a CFL number always less than 0.5 led to correct and smooth transport velocities in every case.

4. NUMERICAL RESULTS

4.1. Validation

In order to validate the present method, the Stokes flow around a circular cylinder between two parallel walls was considered. This problem has been studied both experimentally and theoretically by Bouard and Coutanceau [18]. Here, special attention is given to the product of the Cd number and the Reynolds number and its relationship with the particle diameter to channel width ratio.

In this study, the following dimensionless numbers are defined:

$$\text{Reynolds number: } Re = \frac{\rho_f U_p d_p}{\mu_f}, \quad (18)$$

$$Cd \text{ number: } Cd = \frac{f_x}{\frac{1}{2} \rho_f U_p^2 d_p}, \quad (19)$$

$$\text{Dimensionless diameter: } k = \frac{d_p}{L}, \quad (20)$$

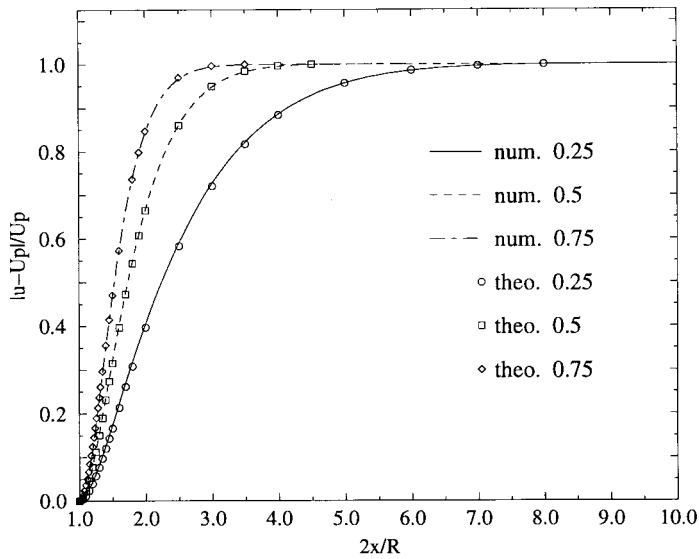


Figure 5. Velocity in front of the cylinder: theoretical and numerical approaches.

where U_p , d_p and L respectively stand for the velocity, the particle diameter and the channel width. In Figure 4, the motion of a particle dragged horizontally with a constant velocity by a body force f_x is presented. The motion is steady. In Figure 4(a)–(c), the streamlines around the particle are displayed. The number of nodes is of the order of 10^4 . One can readily see that the flow is symmetric between the front and the back, and that the particle stays along the middle axis. In the particle itself, the streamlines are parallel, pointing to the fact that it is pseudo-rigid and moves as a solid. In Figure 4(d)–(f), the pressure field is represented. The pressure is defined over the whole domain including the intern of particle. It is continuous at the interface and its maximum value is reached at the stagnation point. In order to compare our results with the theoretical results of Bouard and Coutanceau [18], we have transformed our results so that they are compliant with a Lagrangian frame of reference, that of a fixed particle and moving walls. In Figure 5, a graph representing the variation of the fluid velocity upstream of the particle, along a horizontal line, is presented. As can be readily noted, a good accuracy is obtained everywhere along this line. Bouard [19] has also developed an experimental

Table I. $CdRe$ vs. k

	k	$CdRe$
This study	0.25	44
	0.5	197
	0.75	1710
Bouard <i>et al.</i> [18] (theoretical approach)	0.25	43.95
	0.5	198.9
	0.75	1721
Bouard [19] (experimental approach)	0.25	44
	0.5	196
	0.75	1200

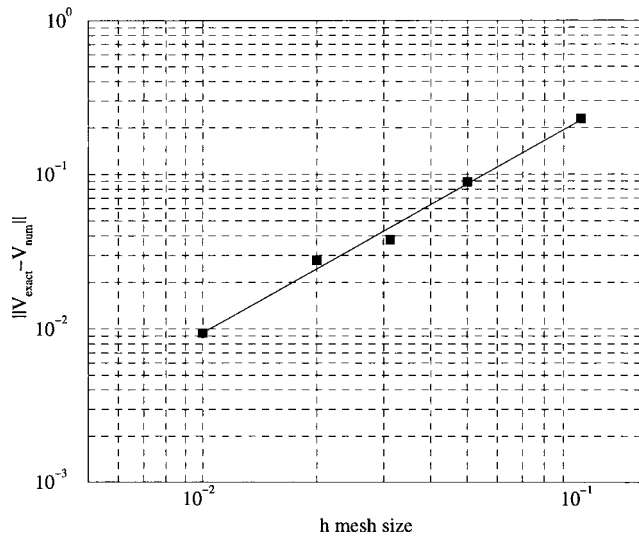


Figure 6. Evolution of the error vs. mesh size h .

approach that can be used to measure the force acting on a moving particle and where the fluid velocity is measured by the so-called particle tracking velocity technique [19]. In Table I, the number $CdRe$ is given for three different particle radii. A good agreement is obtained between the three different approaches. However, when k increases, the experimental error increases strongly [19] and the results of Bouard diverge from those predicted in theory and with our numerical approach. Next, a graph of the velocity L^∞ error with respect to the cell size is presented in Figure 6. What we are looking for is the order of the method, i.e. the value of α in

$$\|\mathbf{V}^{\text{exact}} - \mathbf{V}^{\text{num}}\|_\infty \leq Ch^\alpha, \quad (21)$$

where h , the cell size, varies as the inverse of the number of nodes. The norm $\|\cdot\|_\infty$ is defined as:

$$\|\mathbf{V}^{\text{exact}} - \mathbf{V}^{\text{num}}\|_\infty = \sup_i |\mathbf{V}_i^{\text{exact}} - \mathbf{V}_i^{\text{num}}|, \quad (22)$$

where i stands for the node number. In this work, this error is computed on all nodes upstream of the particle. As can be seen in Figure 6, the method that is proposed in this work is stable and at least linear with respect to the L^∞ norm. More precisely, the value $\alpha = 1.4$ was found.

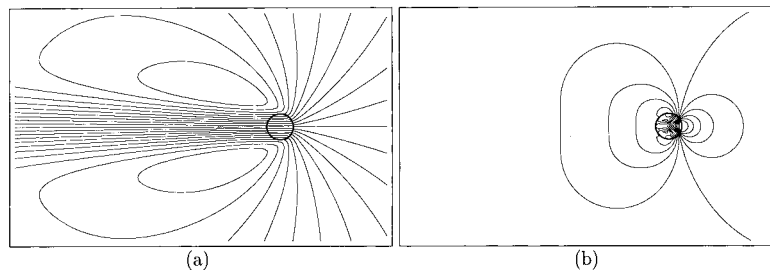


Figure 7. Typical particle motion in an unbounded flow, $Re = 30$: streamlines (a) and isobars (b).

Table II. Drag coefficient vs. Reynolds number

	Re	Drag coefficient
This study	1	11.9
	10	2.72
	20	1.99
	30	1.69
	40	1.51
Bouard [19] (experimental approach)	1	
	10	2.75
	20	2.0
	30	1.7
	40	1.55
Kim <i>et al.</i> [20] (numerical approach)	1	10.325
	10	2.720
	20	1.967
	30	
	40	1.462

We believe that the loss of approximately half of one order of accuracy is imputable to the loss of regularity of the solution at the interface (discontinuous momentum).

In order to study the wake effects during the motion, we calculated the Cd coefficient of a cylinder dragged in an unbounded flow for Reynolds numbers up to 40. Streamlines and

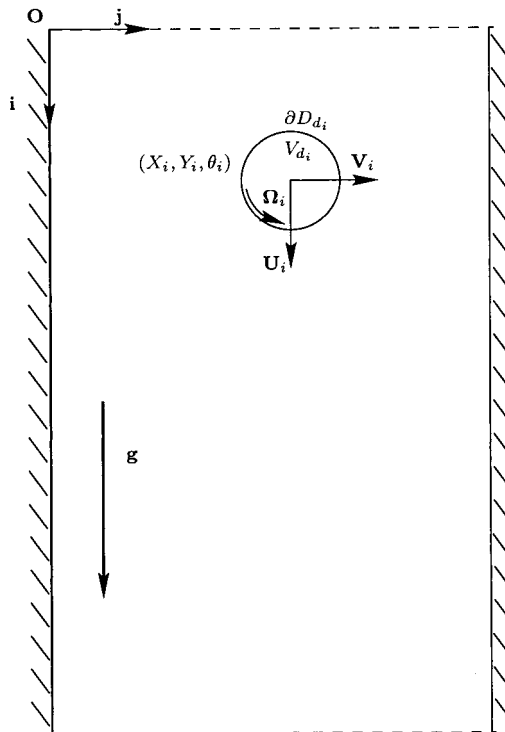


Figure 8. Sedimentation problem.

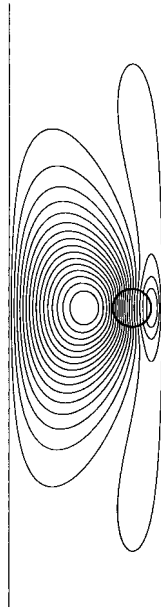


Figure 9. Sedimentation of a circular particle, $Re = 10^{-5}$, $k = 0.25$, streamlines, $\phi_{\min} = -1.8 \times 10^{-8}$, $\phi_{\max} = 1.8 \times 10^{-8}$, $\Delta\phi = 1.8 \times 10^{-9}$.

isobars are shown in Figure 7(a) and (b). Our results were obtained by using a 20000 node rectangular grid. Our results were compared with experimental [19] data and other numerical [20] results. As pointed out in Table II, we observe a good agreement for the drag coefficient. For Reynolds numbers of the order of 100, the method seems to be sufficiently accurate. At higher Reynolds numbers, a thin boundary layer appearing in the neighbourhood of the

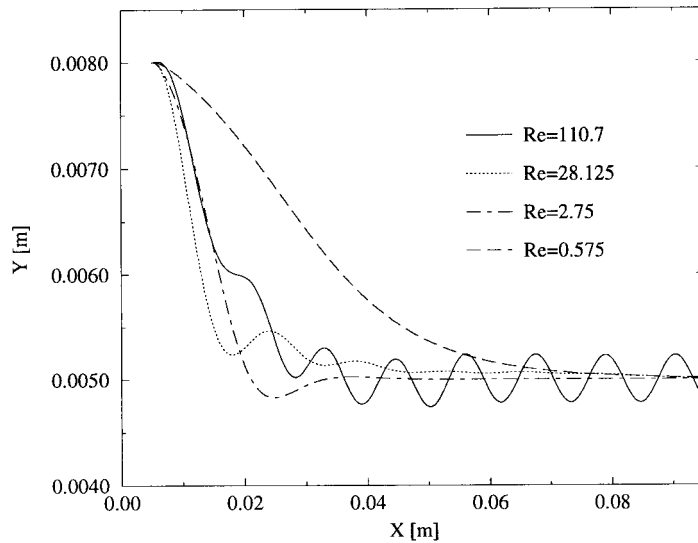


Figure 10. Trajectory of a circular settling particle between two parallel walls for different values of the Reynolds number, $k = 0.25$.

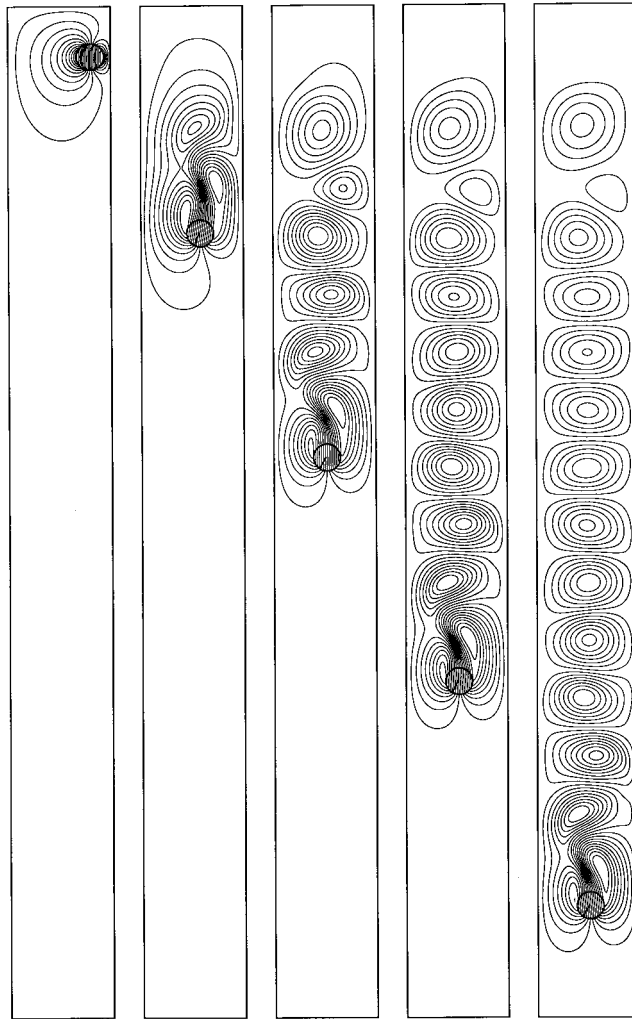


Figure 11. Sedimentation of a circular particle $Re = 110.7$; $k = 0.25$; five positions: $t = 0, 0.5, 1, 1.5, 2$ s; streamlines, $\phi_{\min} = -7 \times 10^{-5}$, $\phi_{\max} = 7 \times 10^{-5}$, $\Delta\phi = 8 \times 10^{-6}$.

surface calls for an increase of the number of nodes in this region. To avoid excessive computational times, it would be convenient to use an adaptative mesh refinement method.

4.2. Numerical study of sedimentation

In this section, the sedimentation of a particle in water is studied. The particle, which is embedded in a closed channel (Figure 8), is assumed to be initially at rest. The Reynolds number that defines the flow conditions is based on the final settling velocity and the diameter of the particle. Different values of the particle density allows us to modify the flow regime. The fluid motion must satisfy a non-slip boundary condition on ∂D :

$$\mathbf{V}|_{\partial D} = \mathbf{0}. \quad (23)$$

Let us mention that, with such a boundary condition, a homogeneous Neumann boundary condition for the Poisson equation is fully justified. In a Stokes regime, when a rigid particle

settles between two parallel walls, the symmetry of the flow (Figure 9) upstream and downstream of this particle leads to a stable trajectory [21]. The particle does not migrate. The distance between its centre and one of the parallel walls remains constant. In an inertia regime, the situation is more complex as pointed out in Figure 10, where the trajectory of the settling particle is displayed for different values of the Reynolds number. Following Feng *et al.* [6] we can observe four different regimes of sedimentation.

- In Stokes flow, the particle does not migrate laterally.
- When the inertia starts playing a role, the velocity and pressure profiles on the surface of the particle become non-symmetric, thereby inducing a transversal force [22,23]. The particle thus migrates towards the walls, and then reaches a stable equilibrium position midway between the two walls.

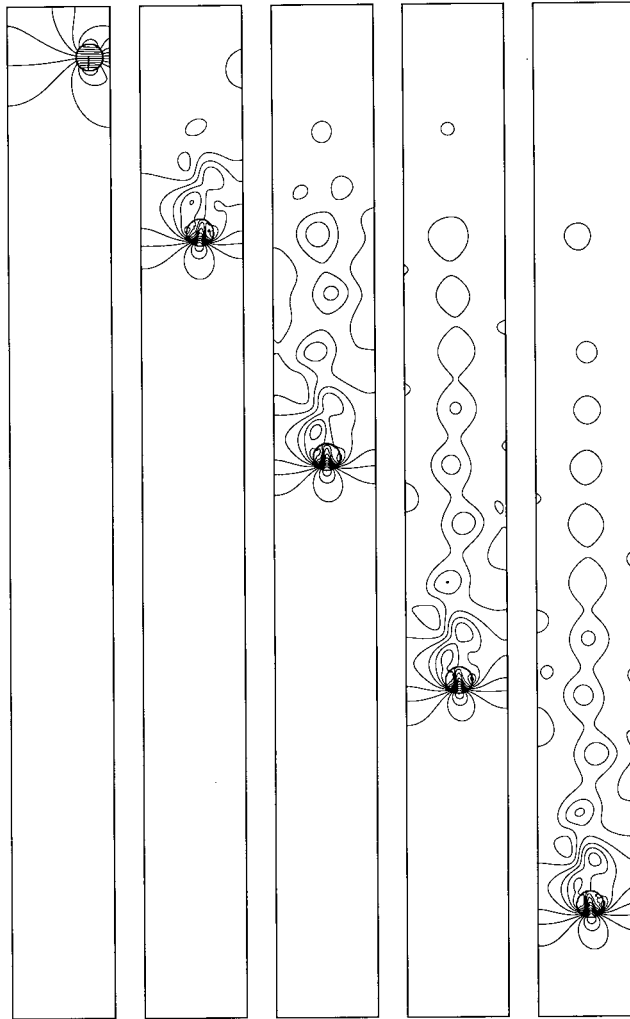


Figure 12. Sedimentation of a circular particle $Re = 110.7$; $k = 0.25$; five positions: $t = 0, 0.5, 1, 1.5, 2$ s; isobars, $p_{\min} = -2$, $p_{\max} = 1.5$, $\Delta p = 0.35$.

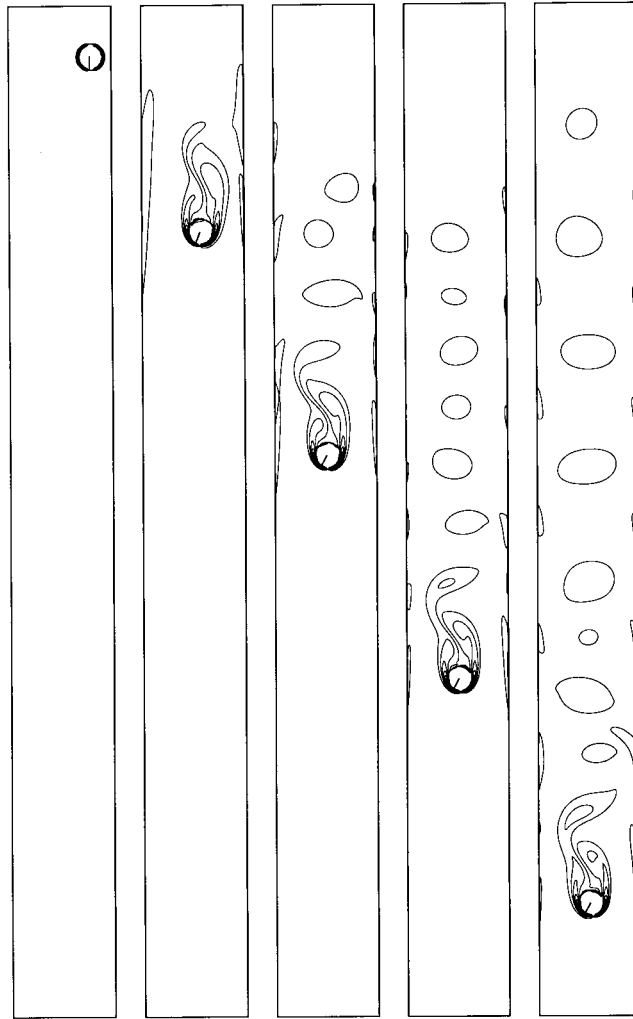


Figure 13. Sedimentation of a circular particle $Re = 110.7$; $k = 0.25$; five positions: $t = 0, 0.5, 1, 1.5, 2$ s, vorticity and angular of particle rotation, $w_{\min} = -320$, $w_{\max} = 28$, $\Delta w = 37.5$.

- At $Re \approx 1$, the formation of a non-symmetric recirculation zone modifies the transverse force so that the particle no longer converges directly to the centre of the domain. Instead, the trajectory oscillates and these oscillations decrease in size as the particle approaches the centre of the canal. The final lateral position is closed to the centre.
- At high values of the Reynolds number, i.e. in the transition regime, the motion becomes inherently unsteady. Even if the velocity tends to a constant value, the recirculation region behind the particle cannot be symmetric and the trajectory of the particle is, therefore, unstable. A zigzagging motion is generated by the oscillating wake behind the particle.

For the sake of illustration, additional results are now presented for $Re = 110.7$. As can be readily seen in Figures 11–13, the wake is unsteady and the action of the flow on the particle perturbs its motion. The particle is moving away from the wall. It is rotating clockwise as if it was rolling up the wall. This phenomenon is called anomalous rolling effect and has been

described by Liu *et al.* [24]. The trajectory fluctuates appreciably. A series of contra-rotating vortices, the size of which is roughly equal to the distance between the two walls, are shed behind the particle which is settling. When the width of the channel is increased, the recirculation grows up as can be seen in Figure 14. At the limit, with no walls, the dissipation of vortices lead to the famous Van Karman vortex shedding.

Finally, we discuss the motion of two settling cylinders between two parallel walls. The cylinders are launched one behind the other and initially the distance between the centres is four diameters. The cylinder that is behind the other one is slightly off-centred to avoid the symmetric non-stable solution. The scenario that appears in such a configuration is called

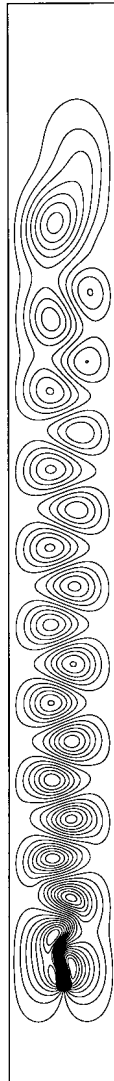


Figure 14. Sedimentation of a circular particle, $Re = 81.25$, $k = 0.125$, $t = 5$ s, streamlines.

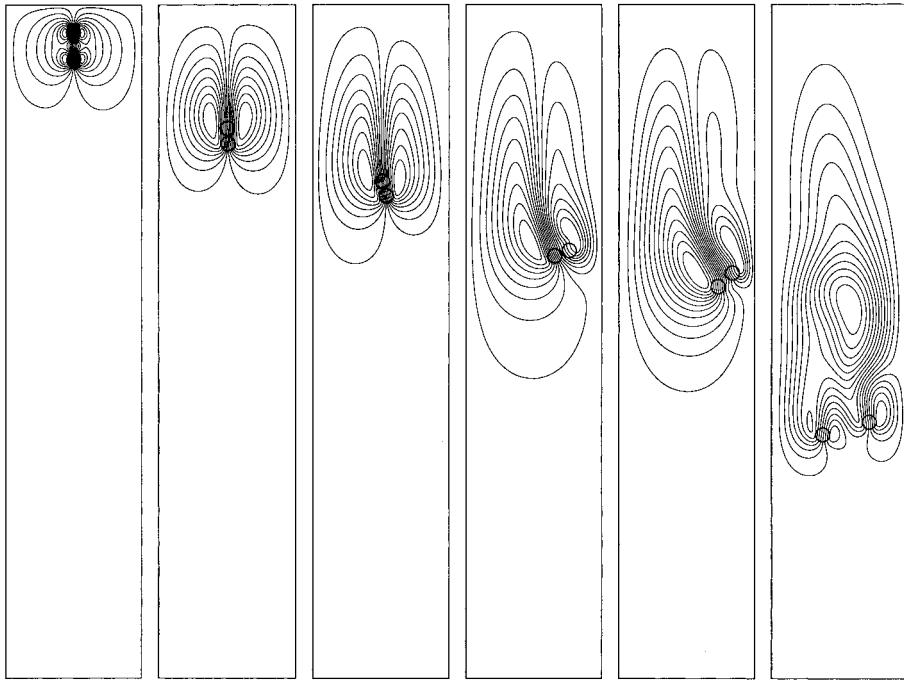


Figure 15. Drafting, kissing, tumbling of two particles, $Re_k = 20$; $k = 0.1$; six positions: $t = 0, 0.532, 0.732, 1.21, 1.32, 2.21$ s; streamlines, $\phi_{\min} = -1.55 \times 10^{-5}$, $\phi_{\max} = 1.55 \times 10^{-5}$, $\Delta\phi = 1.6 \times 10^{-6}$.

drafting, kissing, tumbling (DKT) and was first observed experimentally by Fortes *et al.* [5], and first simulated by Hu *et al.* [3] in two dimensions and later by Johnson *et al.* [8] in three dimensions. The particle behind is carried by the wake triggered by the first particle (drafting), its velocity increases, the distance between the two centres decreases, and eventually there is a contact (kissing). The vertical configuration is unstable and the particles cannot stay one behind the other [25]. The particles are found side by side (tumbling). When kinetic energy is sufficient, the particle behind passes the front particle (see Figure 15). Then the front particle leaves the middle of the channel and is influenced by the fluid that back-flows along the wall. The particle can then stagnate against the wall. In our flow configuration (kissing Reynolds number: $Re_k = 20$), the two particles settle in a stable side by side position after the tumbling position. This configuration was experimentally observed [5]. This mechanism plays a dominant role on the redistribution of the microstructure in the settling suspension because two particles on the same streamlines will be located side by side across streamlines.

4.3. Computational time

It is worthwhile to note that with the proposed method, the computational cost scales linearly with the number of particles [26]. The computational time for one particle in a periodic Poiseuille flow is only 3% more than for no particle. This points to the efficiency of the method. The increase in computational time is imputable only to the calculation of the new position of the particles. Obviously, it would be beneficial to parallelise this procedure. Moreover, the fact that no remeshing and no interpolation are requested at each time step

makes this method a very competitive one. All the computations were performed on Cray computers (C98 and J916). The CPU time depends on the problem size and varied between 15 min and 10 h. The number of scalar nodes was about 10^5 for the simulation in Navier–Stokes regime (note that the computational domain is very long).

As an illustration, this method was used to simulate a two-dimensional sedimentation problem involving as many as 361 particles [26] (Figures 16–21). The initial configuration is a symmetric lattice of 361 particles. We first observe a symmetric sedimentation for a long period of time (Figures 16 and 17). This points out the accuracy of the solver. One must note that, at this time (Figure 17), the line of particles in the middle and at the bottom of the geometry is inherently unstable. Consequently, a small perturbation due to numerical truncature errors may lead to a departure from symmetry in the solution. The redistribution of the microstructure is governed by DKT mechanisms. It is interesting to note that no collision

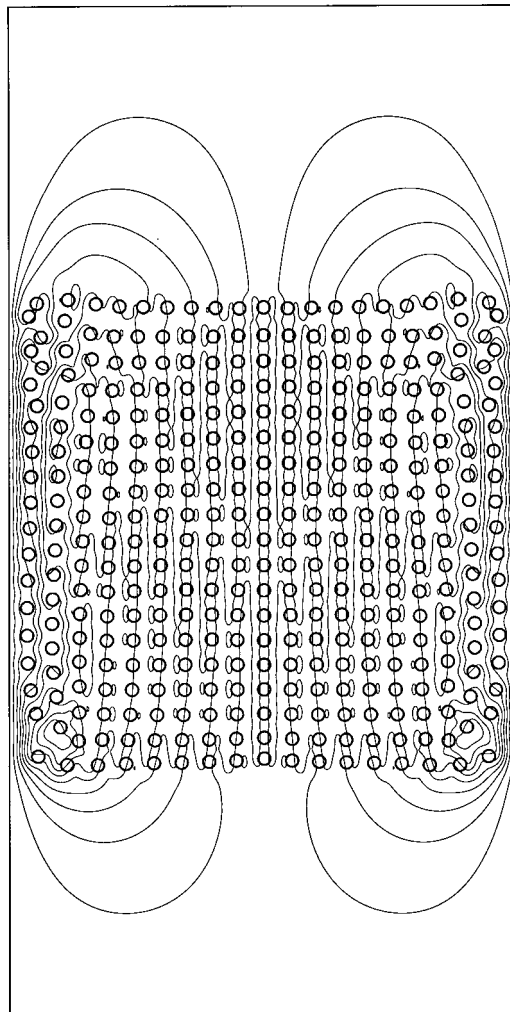


Figure 16. Sedimentation of 361 circular particles between two parallel walls, $Re = 1$, $k = 0.025$, $t = 250$ s, streamlines.

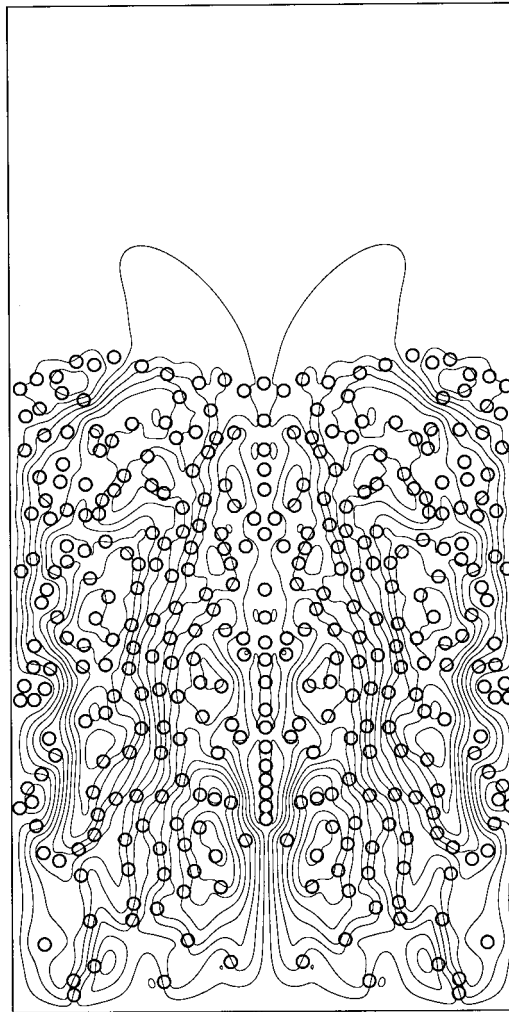


Figure 17. Sedimentation of 361 circular particles between two parallel walls, $Re = 1$, $k = 0.025$, $t = 800$ s, streamlines.

model was considered in this study. In fact, collision does not occur if a suitable time step is chosen. On the figures, the particles are represented as an isosurface of the volume fraction, which explain why two particles may appear overlapped. Finally, after the lack of symmetry has occurred, we observe the sedimentation of particles (Figures 18 and 19) until the deposit of the suspension (Figures 20 and 21).

5. CONCLUSIONS

To conclude, the model we have developed allows the simulation of the transport of rigid particles dispersed in a fluid in an efficient and easy manner. The main characteristic of the

proposed method is to use a very high viscosity to describe the dispersed phase whose behaviour can be assimilated to that of rigid particles. The method is based on a finite volume method, a projection method to solve the momentum equations, a preconditioned bi-conjugated gradient method (BiCGSTAB) to solve the linear systems and an explicit transport of the interfaces between the two phases. The interest of this method is that it needs no remeshing and interpolation of data over the course of a simulation. This leads to a competitive computational cost that scales linearly with the number of particles. Moreover, the properties of the dispersed phases can be defined in a simple manner, which makes it possible to study poly-dispersed phase suspension flows. Presently, the maximum numbers of particles is of the order of 1000 for a two-dimensional problem. The aim of

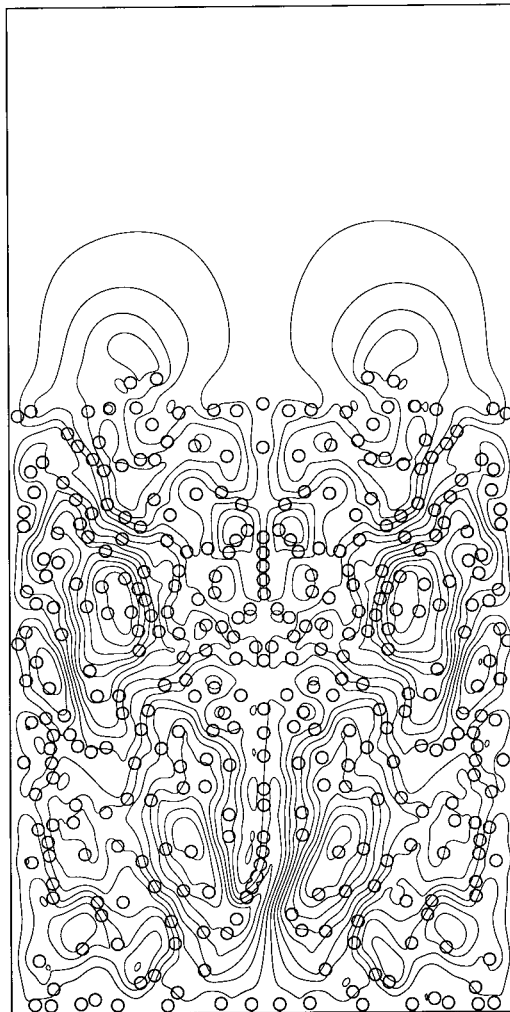


Figure 18. Sedimentation of 361 circular particles between two parallel walls, $Re = 1$, $k = 0.025$, $t = 950$ s, streamlines.

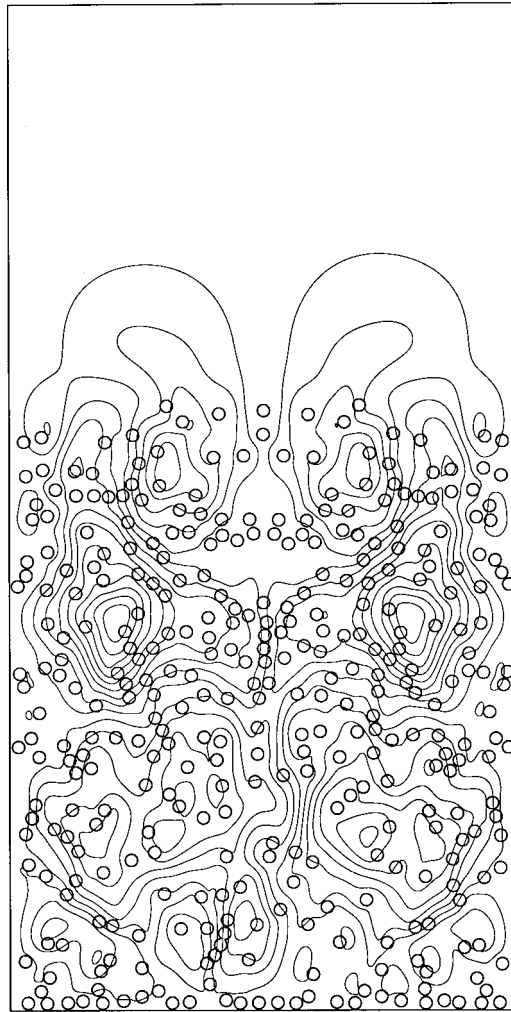


Figure 19. Sedimentation of 361 circular particles between two parallel walls, $Re = 1$, $k = 0.025$, $t = 1050$ s, streamlines.

this direct simulation strategy is to go from a local scale (that of the particles) to a global scale (that of the suspension), and thus be able to access to macroscopic values which can take into account the distorted microstructure governed by the hydrodynamic interactions.

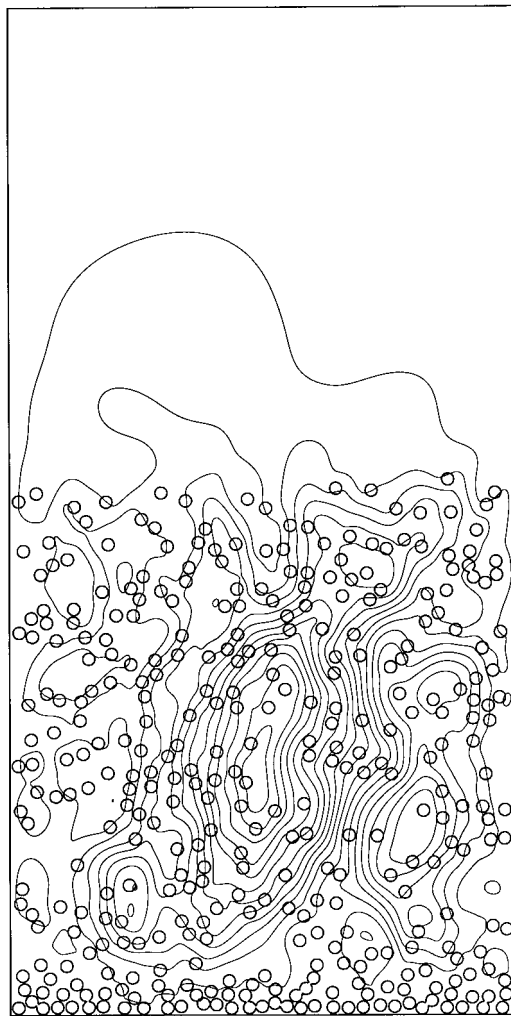


Figure 20. Sedimentation of 361 circular particles between two parallel $Re = 1$, $k = 0.025$, $t = 1300$ s, streamlines.

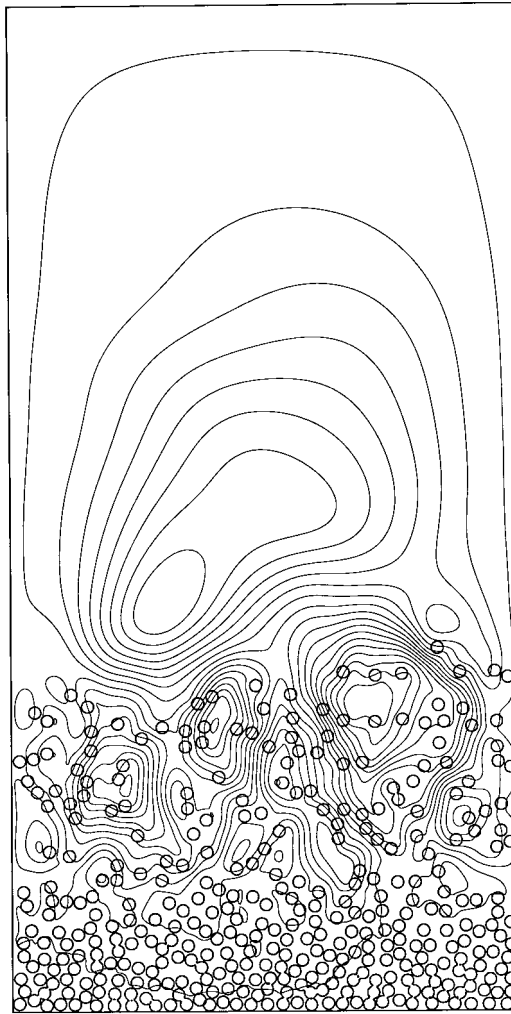


Figure 21. Sedimentation of 361 circular particles between two parallel walls, $Re = 1$, $k = 0.025$, $t = 2000$ s, streamlines.

ACKNOWLEDGMENTS

The authors wish to thank F. Bertrand from the Ecole Polytechnique in Montreal for thoughtful discussions and the reviewers for their suggestions.

REFERENCES

1. C.T. Crowe, T.R. Troutt and J.N. Chung, 'Numerical models for two-phase turbulent flows', *Annu. Rev. Fluid Mech.*, **28**, 11–43 (1996).
2. M.C. Roco, *Particulate Two-Phase Flow*, Butterworth-Heinemann, London, 1993.
3. H.H. Hu, D.D. Joseph and M.J. Crochet, 'Direct simulation of fluid particle motions', *Theoret. Comput. Fluid Dyn.*, **3**, 285–306 (1992).
4. H.H. Hu, 'Direct simulation of flows of solid–liquid mixtures', *Int. J. Multiphase Flow*, **22**, 335–352 (1996).
5. F. Fortes, D.D. Joseph and T.S. Lundgren, 'Non-linear mechanics of fluidization of beds of spherical particles', *J. Fluid Mech.*, **177**, 467–483 (1987).

6. J. Feng and D.D. Joseph, 'The unsteady motion of solid bodies in creeping flows', *J. Fluid Mech.*, **303**, 83–102 (1995).
7. J. Feng, H.H. Hu and D.D. Joseph, 'Direct simulation of initial value problems for the motion of solid bodies in a Newtonian fluid, Part 1. Sedimentation', *J. Fluid Mech.*, **261**, 95–134 (1994).
8. A.A. Johnson and T.E. Tezduyar, 'Simulation of multiple spheres falling in a liquid-filled tube', *Comput. Methods Appl. Mech. Eng.*, **134**, 351–373 (1996).
9. A.A. Johnson and T.E. Tezduyar, '3D simulation of fluid–particle interactions with the number of particles reaching 100', *Comput. Methods Appl. Mech. Eng.*, **145**, 301–321 (1997).
10. T.E. Tezduyar, M. Behr and J. Liou, 'A new strategy for finite element computations involving moving boundaries and interfaces—the deforming spatial domain/space–time procedure: I. The concept and the preliminary tests', *Comput. Methods Appl. Mech. Eng.*, **94**, 339–351 (1992).
11. R. Glowinsky, T. Hesla, D.D. Joseph, T.W. Pan and J. Periaux, in M.O. Bristeau, G. Etgen, W. Fitzgibbon, J.L. Lions, J. Periaux and M.F. Wheeler (eds.), *Distributed Lagrange Multiplier Methods for Particulate Flows, Computational Science for the 21st Century*, Wiley, Chichester, 1997, pp. 270–279.
12. F.H. Harlow and J.E. Welch, 'Numerical calculation of time dependent viscous incompressible flow', *Phys. Fluids*, **8**, 21–82 (1965).
13. K. Goda, 'A multistep technique with implicit difference schemes for calculating two- or three-dimensional cavity flows', *J. Comput. Phys.*, **30**, 76–95 (1979).
14. A.J. Chorin, 'A numerical method for solving incompressible viscous flow problems', *J. Comput. Phys.*, **2**, 12–26 (1967).
15. B.P. Leonard, 'A stable and accurate convective modelling procedure based on quadratic upstream interpolation', *Comput. Methods Appl. Mech. Eng.*, **19**, 59–98 (1979).
16. S.V. Patankar, *Numerical Heat Transfer and Fluid Flow*, Hemisphere, New York, 1990.
17. H.A. Van der Vorst, 'A fast and smoothly converging variant of Bi-CG for the solution of non-symmetric linear systems', *SIAM, J. Sci. Stat. Comput.*, **13**, 631–644 (1992).
18. R. Bouard and M. Cousteau, 'Etude théorique et expérimentale de l'écoulement engendré par un cylindre en translation uniforme dans un fluide visqueux en régime de Stokes', *J. Appl. Math. Phys.*, **37**, 673–684 (1986).
19. R. Bouard, 'Etude de l'écoulement autour d'un cylindre soumis à une translation uniforme après un départ impulsif, pour des nombres de Reynolds allant de 0 à 10^4 ', *Thèse d'État*, Université de Poitiers, 1983.
20. D.W. Kim and M.U. Kim, 'Minimum drag shape in two-dimensional viscous flow', *Int. J. Numer. Methods Fluids*, **21**, 93–111 (1995).
21. J. Happel and H. Brenner, *Low Reynolds Number Hydrodynamics*, Kluwer Academic, Dordrecht, 1983.
22. B.P. Ho and L.G. Leal, 'Inertial migration of rigid spheres in two-dimensional unidirectional flows', *J. Fluid Mech.*, **65**, 365–400 (1974).
23. L.G. Leal, 'Particle motions in a viscous fluid', *Annu. Rev. Fluid Mech.*, **12**, 435–477 (1980).
24. Y.J. Liu, J. Nelson, J. Feng and D.D. Joseph, 'Anomalous rolling of spheres down an inclined plane', *J. Non-Newtonian Fluid Mech.*, **50**, 305–329 (1993).
25. P.Y. Huang, J. Feng and D.D. Joseph, 'The turning couples on an elliptic particle settling in a vertical channel', *J. Fluid Mech.*, **271**, 1–16 (1994).
26. J.B. Ritz, 'Modélisation des écoulements fluide-particules', *Thèse*, Université de Bordeaux I, 1997.